Chemical Engineering Journal 329 (2017) 56–65

Contents lists available at ScienceDirect

Chemical Engineering Journal

journal homepage: www.elsevier.com/locate/cej

Method for generating pore networks in porous particles of arbitrary shape, and its application to catalytic hydrogenation of benzene

Guanghua Ye [a], Yuanyuan Sun [a], Xinggui Zhou [a,*], Kake Zhu [a], Jinghong Zhou [a], Marc-Olivier Coppens [b,*]

[a] State Key Laboratory of Chemical Engineering, East China University of Science and Technology, Shanghai 200237, China
[b] Department of Chemical Engineering, University College London, London WC1E 7JE, UK

HIGHLIGHTS

- An adaptable, efficient pore network cutting algorithm is proposed.
- Pore networks with 8 archetypical shapes are successfully built as examples.
- Pore networks are applied to simulate diffusion and reaction in porous catalysts.
- Shape and randomness of the pore network could affect catalytic performance.
- A larger effectiveness factor of catalysts is found for a regular pore network.

GRAPHICAL ABSTRACT

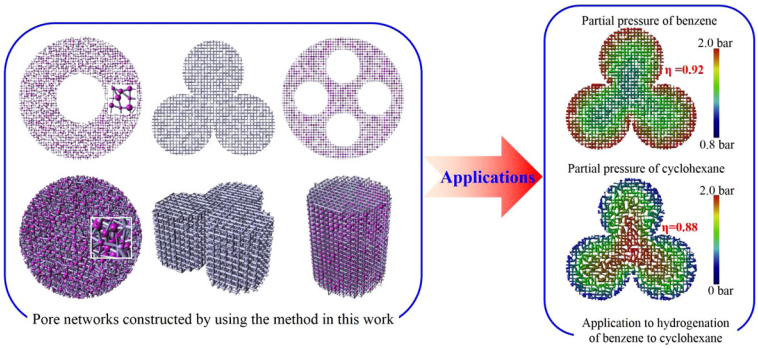

ARTICLE INFO

Article history:
Available online 16 February 2017

Keywords:
Porous materials
Pore network
Particle shape
Cutting algorithm
Hydrogenation of benzene
Catalysis

ABSTRACT

A method is established to generate pore networks within domains of arbitrary shape, as long as the domain can be mathematically described by a set of inequalities. In this method, a stochastic network algorithm is adopted to construct pore network skeletons, which are then cut into the desired shapes using a new pore network cutting algorithm. The latter can be embedded into other methods to transplant its 'pore network cutting' function. Using this method, pore networks with four archetypical two-dimensional shapes (namely, cross-sections of one-holed rings, trilobes, four-holed rings, and wheels) and four three-dimensional shapes (namely, spheres, cylinders, trilobes, and hollow cylinders) are constructed as examples. Then, some of these pore networks are applied to simulate diffusion and reaction in Pd/γ-alumina catalyst particles for hydrogenation of benzene to cyclohexane. It is shown that the randomness of the pore network and the external particle shape significantly affect the performance of catalysts, because of their impact on effective diffusivity and diffusion length, respectively, indicating that this structural information must be accounted for to achieve a model with high accuracy. The versatile method proposed in this article is ideal to study the effect of particle shape and pore network structure on the performance of porous materials for catalysis and other applications.

1. Introduction

Porous materials are widely used in the chemical industry as catalysts, adsorbents, membranes, etc. Such materials contain a huge number of pores of different geometry and size, which are interconnected to form networks of different topology. In addition,

* Corresponding authors.
E-mail addresses: xgzhou@ecust.edu.cn (X. Zhou), m.coppens@ucl.ac.uk (M.-O. Coppens).

http://dx.doi.org/10.1016/j.cej.2017.02.036
1385-8947/

these materials come in various shapes, depending on their applications. External shape, pore morphology and pore network topology can all strongly affect the overall properties of porous materials [1–4]. Therefore, accurate pore network representations are essential for porous material characterization and design.

Many types of pore models have been conceived to describe porous materials; these have been reviewed by Sahimi et al. [5] and Keil [6]. Early models include the parallel pore model, tortuous pore model, cylindrical pore model, model of Wakao and Smith, and grain model. Although these early models could describe certain features of the pore space (pore size distribution, porosity, and, to some extent, tortuosity) and could be extended to account for morphological features like pore surface roughness, they do not explicitly account for the pore network topology or pore connectivity, or for the spatial distribution of the pores. Compared to these early models, pore network models are more representative of the pore space [7,8]. At present, pore networks are frequently used to represent the pore space of rocks [9,10], adsorbents [11], membranes [12–14], fuel cell electrodes [15–17], and porous catalysts [18–21].

Pore networks can be generated by using regular lattice-based, stochastic, and image-based methods [22–24]. Bethe lattices with a connectivity of 3 or more, square lattices with a connectivity of 4, and cubic lattices with a connectivity of 6 have been employed to build lattice-based pore networks. The connectivity can be altered by removing or adding bonds. The pore size is assigned according to some statistical distribution, such as the Gaussian distribution. Although some irregularities can be introduced in the lattice-based pore networks by varying the position of sites, these pore networks are not adequate to describe irregular pore network structures. Stochastic pore networks are better suited in this case. Normally, sites are randomly or uniformly distributed in a square domain or a cubic domain; then, adjacent sites are interconnected according to connectivity; shapes and sizes of sites and bonds are assigned in the final step. Finally, image-based pore networks are extracted from the three-dimensional (3-D) images that can be obtained by using statistical methods, process-based methods, and X-ray micro-tomographic characterization [25]. Although this image-based method yields pore networks closest to the real porous materials, this method is computationally intensive and

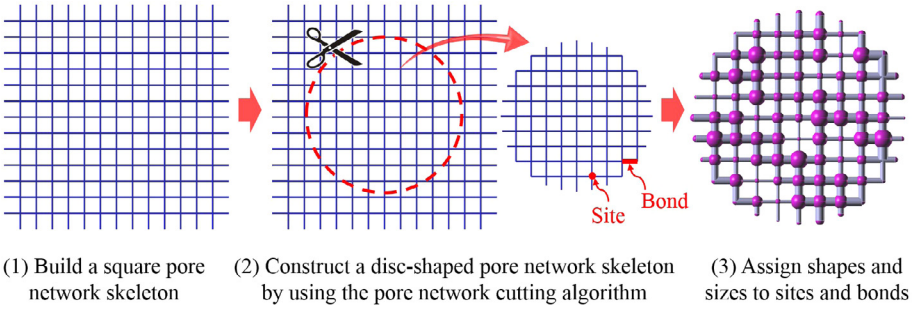

Fig. 1. Schematic illustrating how to generate a disc-shaped pore network. In this illustration, a regular network is given as an example, however, this method is actually applicable to any network, including irregular ones.

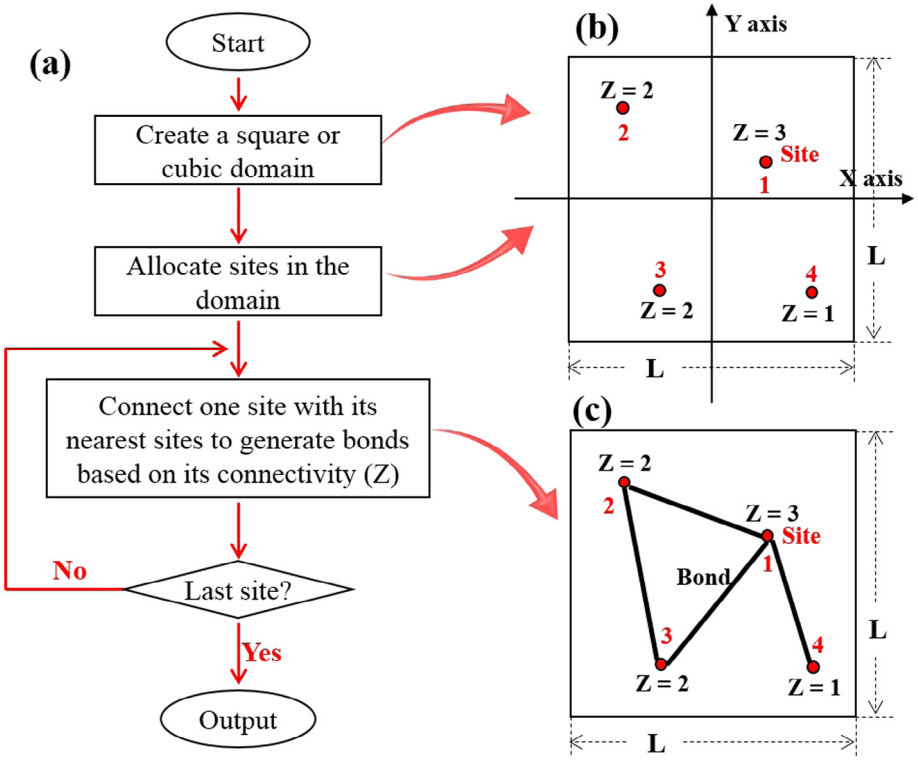

Fig. 2. (a) Flowchart for the stochastic network algorithm; (b)–(c) a 2-D illustration for the algorithm.

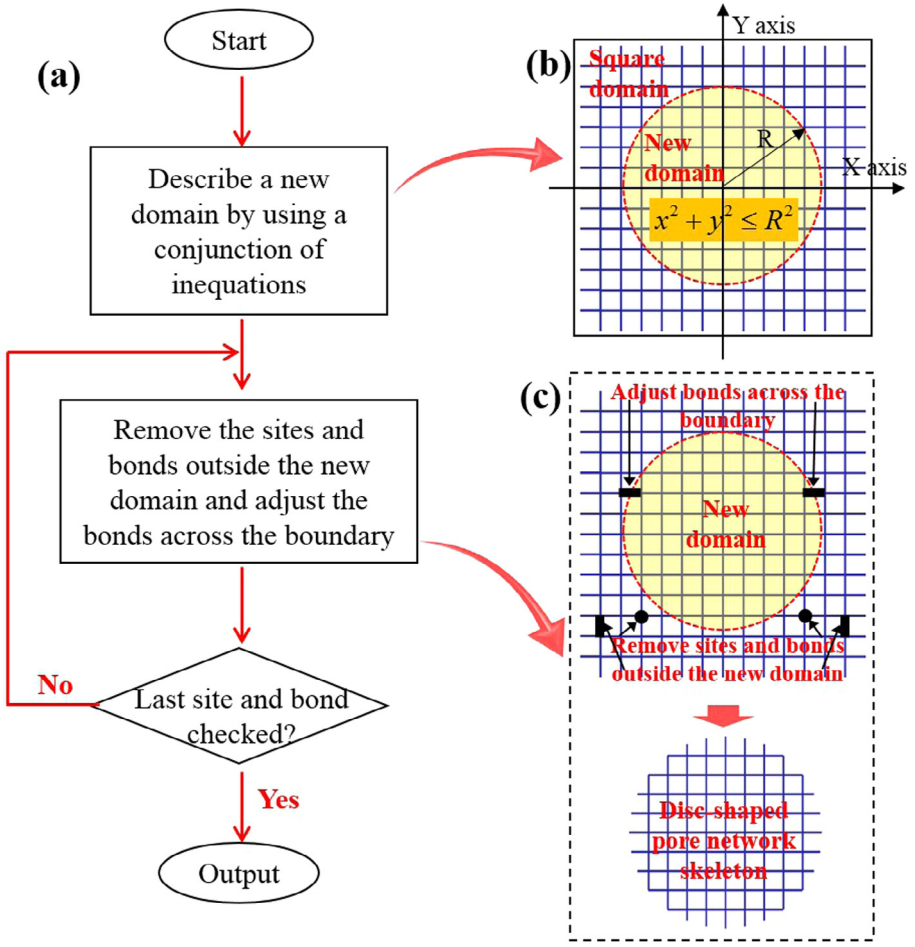

Fig. 3. (a) The flowchart for the pore network cutting algorithm; (b)–(c) a 2-D illustration of the algorithm.

Table 1
Parameters for generating the pore networks in Section 3 (arbitrary units of length).

T1 pore networks	
Standard deviation of pore size distribution (σ_p)	0.05
Volume-averaged pore radius (r_{pa})	0.15
Lower limit of pore radius (r_{pl})	0.05
Upper limit of pore radius (r_{pu})	0.25
T2 pore networks	
Standard deviation of pore size distribution (σ_p)	0.10
Volume-averaged pore radius (r_{pa})	0.25
Lower limit of pore radius (r_{pl})	0.10
Upper limit of pore radius (r_{pu})	0.40
Standard deviation of throat size distribution (σ_t)	0.03
Volume-averaged throat radius (r_{ta})	0.10
Lower limit of throat radius (r_{tl})	0.05
Upper limit of throat radius (r_{tu})	0.15

involves complicated network extraction algorithms, such as the thinning algorithm [26], the medial axis based algorithm [27,28], and the maximal ball algorithm [29,30].

The three methods mentioned above are mainly used to generate square and cubic pore networks, and not designed to build pore networks of arbitrary shape. Up to now, a method for generating pore networks of arbitrary shape has not been reported in the literature.

Constructing pore networks of arbitrary shape is of industrial importance. The porous materials used in the chemical industry usually have different shapes. The shape of porous materials can significantly affect mass transfer in them, flow around them, and their mechanical strength. Mohammadzadeh and Zamaniyan [31] evaluated the effect of particle shape on the performance of catalysts for steam reforming of methane. They found that the catalyst effectiveness decreases with particle shape in the order: hollow cylinders > cylinders > spheres. Brunner et al. [32] obtained the same result for Fischer-Tropsch synthesis catalysts. Brunner et al. [32] also reported that the pressure drop of a fixed-bed reactor can be significantly reduced by using trilobes instead of spheres. Šolcová and Schneider [33] and Šolcová et al. [34] investigated the effect of particle shape on the axial dispersion in a column packed with porous particles. They found that, besides the particle size, the particle shape significantly affects the axial dispersion. Wu et al. [35] evaluated the mechanical properties of porous particles with different shapes. They observed that a trilobe particle is easier to break than a cylindrical particle under mechanical stress. The most suitable particle shape depends on the application. Therefore, a method for building pore networks of arbitrary shape is very useful in evaluating or designing industrial porous materials, especially porous catalysts.

In this article, we propose a method to generate pore networks of arbitrary shape. The algorithms involved in this method are described, and some archetypical shapes, which are commonly used in the chemical industry, are constructed as examples. After that, some pore networks are applied to simulate hydrogenation of benzene to cyclohexane in catalyst particles, and the effects of pore-network randomness and external shape on the performance of catalysts are studied.

2. Methodology

The method consists of three steps: (1) building an original pore network skeleton within a square or cubic domain (the details are explained in Section 2.1), (2) changing this original skeleton into a new skeleton of the desired shape by using the pore network cutting (PNC) algorithm proposed in this work, (3) assigning geometrical information (shapes and sizes) to sites and bonds. Fig. 1 illustrates these procedures with a 2-D example. The key, new step is using the PNC algorithm.

2.1. Generating original pore network skeletons

A stochastic network algorithm [36] is employed to generate original pore network skeletons. The flowchart of this algorithm is presented in Fig. 2a, and a 2-D illustration for this algorithm is also given in Fig. 2b and c. A detailed description is as follows:

(1) Establish a 2-D (X, Y) or 3-D (X, Y, Z) Cartesian coordinate system, and define a square ($L \times L$) or cubic ($L \times L \times L$) domain with the origin in the center and the edges parallel to one axis.
(2) Place sites within the domain regularly or irregularly as desired, label all these sites, and assign connectivity (Z) to each site. The number of sites determines the size of the pore network skeleton. In this work, the connectivity is 4 for 2-D pore networks and 6 for 3-D ones.
(3) Start with the site No.1 and connect this site with its adjacent sites to generate bonds, according to the connectivity. Then move to the next site and do the same thing, which is repeated until the last site has been well connected. It is worth noting that the solution can be different, depending on the order in which the sites are selected.
(4) Output the data of the original pore network skeleton.

2.2. Pore network cutting algorithm

The PNC algorithm is proposed to change the original pore network skeleton into a desired shape. The flowchart of this PNC algorithm is shown in Fig. 3a. It consists of the following steps:

(1) Describe the new domain of a desired shape by using a set of inequalities.
(2) Remove the sites and bonds outside the new domain, and adjust the bonds across the domain boundary by breaking these bonds on the boundary and then removing their parts outside the new domain. This step is repeated until the last site and bond have been checked.
(3) Output the data of the pore network skeleton with a desired shape.

With the PNC algorithm, the original pore network skeleton can be 'cut' into arbitrary shapes, as long as these shapes can be mathematically described by a set of inequalities. The skeleton can be reused as often as necessary, which reduces the computational cost significantly when pore networks within domains of many different shapes need to be generated. Besides, this PNC algorithm can be embedded into other methods for pore network generation to transplant its 'pore network cutting' function.

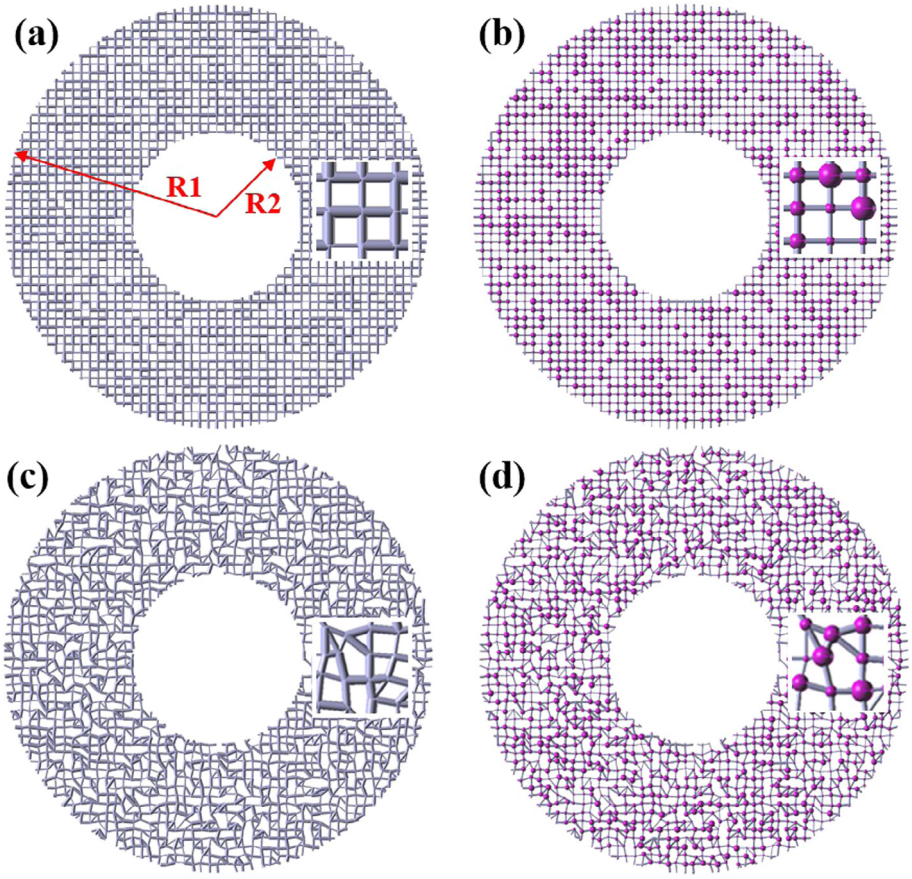

Fig. 4. (a) T1R 2-D one-holed ring pore network, (b) T2R 2-D one-holed ring pore network, (c) T1IR 2-D one-holed ring pore network, (d) T2IR 2-D one-holed ring pore network. The details of these pore networks are shown in the insets.

2.3. Assigning shapes and sizes to sites and bonds

Two types (T1 and T2) of pore networks are generated in this work. For T1, the sites are treated as zero-volume intersections and the bonds are replaced by cylindrical pores; the pore radius is randomly assigned to each pore according to a statistical pore size distribution. For T2, the sites and bonds are replaced by spherical pores and cylindrical throats, respectively. The pore radius and throat radius are allocated according to a statistical pore size distribution and throat size distribution, and the radius of each pore should be larger than the radii of the throats connected with this pore [36]. It is worth noting that the radius of a pore on the boundary is assumed to be the radius of one throat connected with this pore; this assumption would not affect most applications of the pore networks.

In this work, pore radius (r_p) and throat radius (r_t) are dimensionless and follow a modified Gaussian distribution [37], as described by Eq. (1):

$$f(r) = \frac{\frac{1}{\sqrt{2\pi}\sigma}\exp\left[-\frac{(r-r_a)^2}{2\sigma^2}\right]}{\int_{r_l}^{r_u}\frac{1}{\sqrt{2\pi}\sigma}\exp\left[-\frac{(r-r_a)^2}{2\sigma^2}\right]dr} \quad r_l \leqslant r \leqslant r_u \tag{1}$$

where σ is the standard deviation, r_a is the volume-averaged radius, and r_l and r_u are the lower and upper limits of the radius. Table 1 shows the parameters used to construct the T1 and T2 pore networks in Section 3.

The algorithms of this method are implemented in MATLAB 2010b, and these pore networks are displayed by using Rhinoceros 4.0. On a Dell desktop with a 3.06 GHz Intel Core i3 CPU and 4 GB of RAM, it takes 8 min to construct an original square pore network skeleton with 2601 sites and 16 min to construct a cubic one with 15,625 sites, but only several seconds to "cut" this original pore network into a desired shape.

3. Results

3.1. Two-dimensional pore networks

The original square pore network skeleton (domain size: 50×50, dimensionless) holds 2601 sites, which are regularly or irregularly distributed. Using this skeleton, 2-D pore networks with four archetypical shapes (namely, cross-sections of one-holed rings, trilobes, four-holed rings, and wheels) of industrial catalysts are generated as examples. Four groups of pore networks are constructed, namely: T1 pore network with sites regularly distributed (T1R), T1 pore network with sites irregularly distributed (T1IR), T2 pore network with sites regularly distributed (T2R), and T2 pore network with sites irregularly distributed (T2IR). To avoid repetition, only 2-D one-holed ring pore networks and 2-D trilobe pore networks are shown in this section, while the other pore networks are presented in the Supporting Information.

Fig. 4 shows 2-D one-holed ring pore networks, and the 2-D one-holed ring domain can be described by a set of inequalities:

$$\begin{cases} x^2 + y^2 \leqslant R_1^2 \\ \quad AND \\ x^2 + y^2 \geqslant R_2^2 \end{cases} \tag{2}$$

where R_1 and R_2 are the radii of the outer circle and the inner circle, respectively.

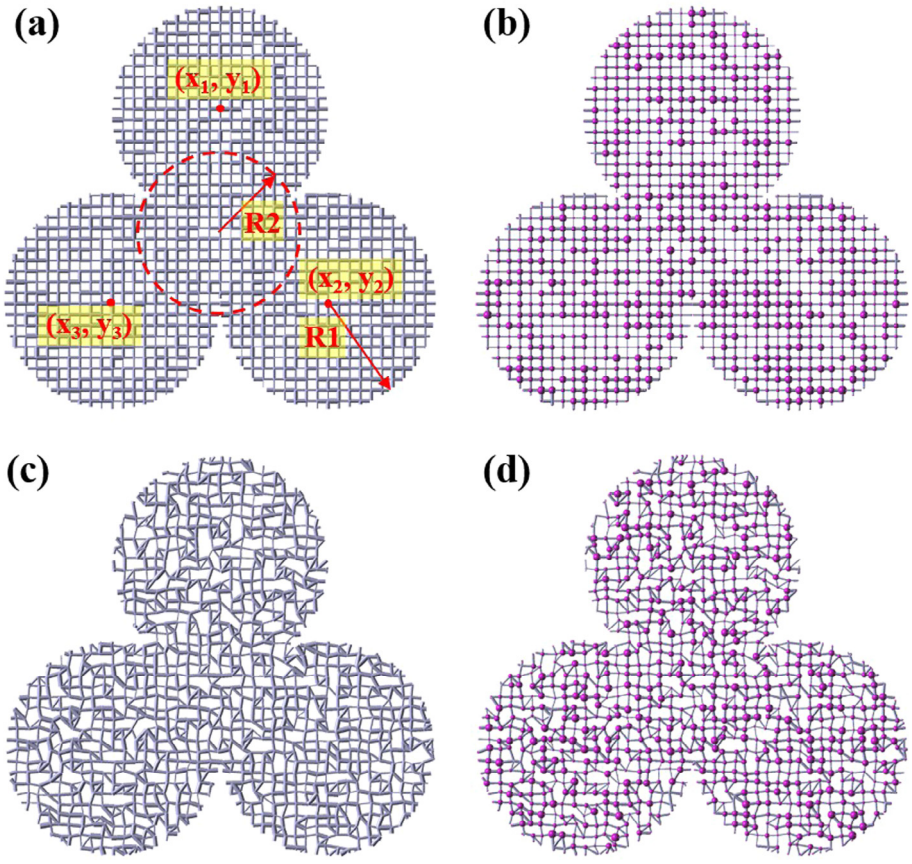

Fig. 5. (a) T1R 2-D trilobe pore network, (b) T2R 2-D trilobe pore network, (c) T1IR 2-D trilobe pore network, (d) T2IR 2-D trilobe pore network.

Fig. 5 shows 2-D trilobe pore networks; the corresponding domain is formed by merging one central circle and three circles around it, overlapping with this central circle:

$$\begin{cases} x^2+y^2 \leqslant R_2^2 \\ \quad OR \\ (x-x_1)^2+(y-y_1)^2 \leqslant R_1^2 \\ \quad OR \\ (x-x_2)^2+(y-y_2)^2 \leqslant R_1^2 \\ \quad OR \\ (x-x_3)^2+(y-y_3)^2 \leqslant R_1^2 \end{cases} \tag{3}$$

where R_2 is the radius of the center circle; (x_1, y_1), (x_2, y_2), and (x_3, y_3) are the center coordinates of the three other circles with radius R_1.

3.2. Three-dimensional pore networks

The original cubic pore network skeleton (domain size: $24 \times 24 \times 24$, dimensionless) holds 15,625 sites. With this original skeleton, 3-D pore networks with four archetypical shapes (i.e., sphere, cylinder, trilobe, and hollow cylinder) are constructed as examples, and four groups (T1R, T1IR, T2R, and T2IR) of pore networks are presented. To avoid repetition, only pore networks within the sphere and the cylinder are shown in this section, while the other pore networks are presented in the Supporting Information.

Fig. 6 shows pore networks within a spherical domain that is described by the inequality:

$$x^2+y^2+z^2 \leqslant R^2 \tag{4}$$

where R is the radius of the sphere.

Fig. 7 shows pore networks within a cylindrical domain that is described by the following set of inequalities:

$$\begin{cases} x^2+y^2 \leqslant R^2 \\ \quad AND \\ Z \leqslant 0.5L \\ \quad AND \\ Z \geqslant -0.5L \end{cases} \tag{5}$$

where R is the radius of the cylinder, and L is the axial length.

4. Application to hydrogenation of benzene

4.1. Modelling of diffusion and reaction in the catalyst particles

Some of the T1 pore networks built in this work are applied to simulate hydrogenation of benzene to cyclohexane in Pd/γ-alumina catalyst particles with various shapes. Gas-phase diffusion and reaction are simulated using a pore network model, which is similar to the one in our previous papers [20,21], therefore, only the principal equations are given here. For the cylindrical pore n, the continuity equation for component i is:

$$\frac{dJ_{i,n}}{dl_n}\frac{r_n}{2} - R_i = 0 \tag{6}$$

where $J_{i,n}$ is the diffusion flux of component i in pore n, l_n and r_n are the length and the radius of pore n, R_i is the reaction rate per pore surface area of component i. For an inner site, Kirchhoff's law is employed:

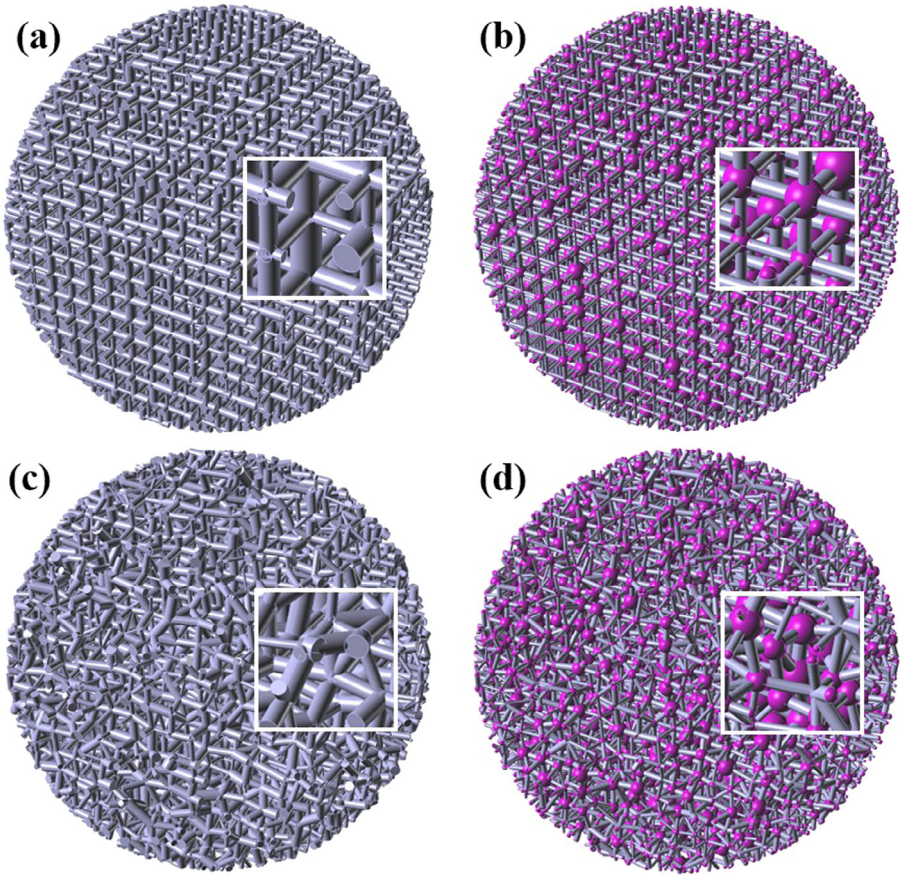

Fig. 6. (a) T1R pore network, (b) T2R pore network, (c) T1IR pore network, (d) T2IR pore network within a sphere. The details of these pore networks are shown in the insets.

$$\sum_{n=1}^{n=Z} \pi r_n^2 J_{i,n} = 0 \tag{7}$$

where Z is the pore network connectivity. For the boundary site m, a Dirichlet boundary condition is assumed:

$$C_{i,m} = C_{i,b} \tag{8}$$

where $C_{i,m}$ is the concentration of component i in site m and $C_{i,b}$ is the bulk concentration of component i.

The parameters for the simulations in Sections 4.2 and 4.3 are presented in Table 2. If the partial pressure of benzene and cyclohexane are high or the temperature is low, capillary condensation can occur in the catalyst particles, which would make the pore network modeling substantially more difficult, but can be done using the same networks provided in this paper. To avoid this additional complication, the pressure and temperature in Table 2 are chosen such that all components in the catalyst particles are in the vapor phase. In practice, for the same reaction, the catalyst particles loaded in a fixed-bed reactor can be completely dry, i.e., only vapor-filled [38,39]. Finally, Eqs. (6)-(8) are simultaneously and iteratively solved by using the function 'fsolve' in Matlab, and the computation time is 1.5 min for a pore network with 1152 sites. It is worth mentioning that the numbers of sites adopted in Section 4 are reasonable, because the simulation results are almost the same, but the computing cost increases significantly when adding more sites, even though these numbers of sites result in artificially long pores [20].

4.2. Effect of pore-network randomness

By using T1R and T1IR 2-D pore networks within a trilobe-shaped domain (R_1 = 2.5 mm, R_2 = 1.5 mm, see Fig. 5a and c), the effect of pore-network randomness on the performance of the catalyst particles is investigated. The partial pressure gradients of benzene and cyclohexane in the T1R network are smaller than the ones in the T1IR network, so that the effectiveness factor for the T1R network (η = 0.92) is larger than the one for the T1IR network (η = 0.88), as shown in Fig 8. These results indicate that pore-network randomness can affect the performance of catalysts, and the catalysts with regular pore network perform better.

The irregular pore network has more tortuous diffusion paths [40] and, therefore, the effective diffusivities of all components

Table 2
Parameters for simulating hydrogenation of benzene to cyclohexane in the catalyst particles.

Standard deviation (σ_p)	2.0
Volume-averaged pore radius (r_{pa})	3.5 nm
Lower limit of pore radius (r_{pl})	1.0 nm
Upper limit of pore radius (r_{pu})	6.0 nm
Pore network connectivity (Z)	4 (2-D), 6 (3-D)
Partial pressure of benzene in the bulk ($P_{B,b}$)	2 bar
Partial pressure of hydrogen in the bulk ($P_{H,b}$)	8 bar
Partial pressure of cyclohexane in the bulk ($P_{C,b}$)	~0 bar
Total pressure (P_t)	10 bar
Temperature (T)	433 K

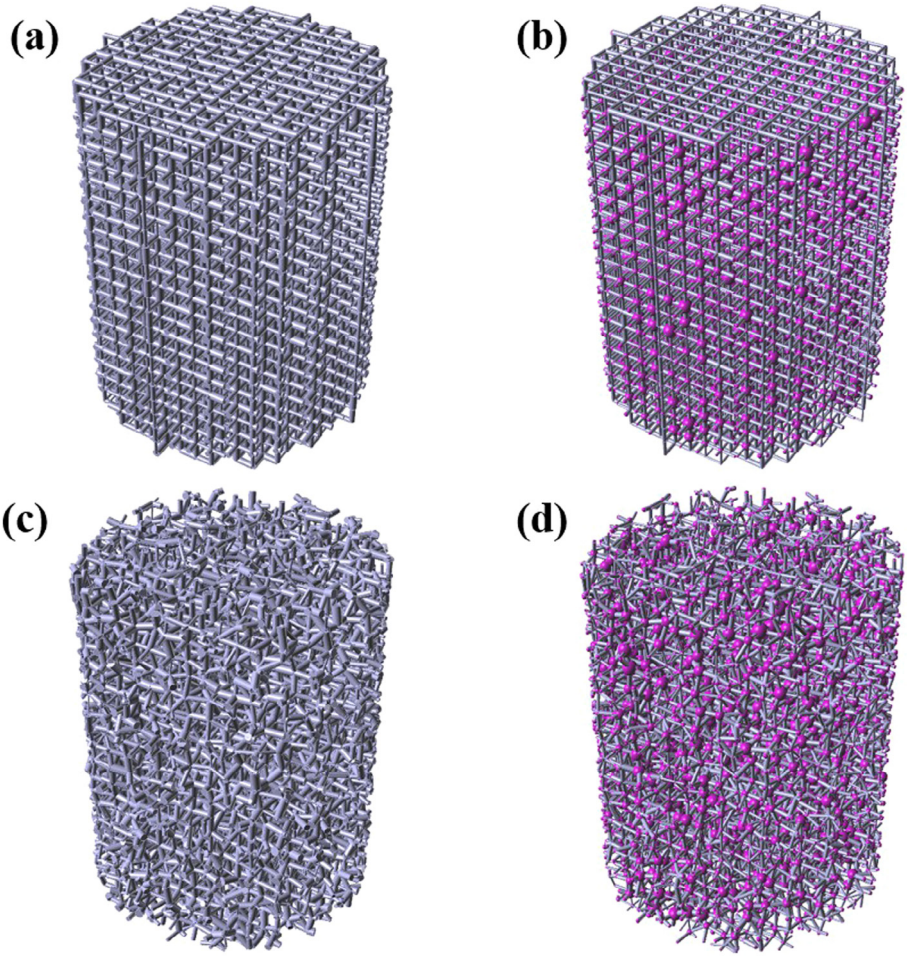

Fig. 7. (a) T1R pore network, (b) T2R pore network, (c) T1IR pore network, (d) T2IR pore network within a cylindrical domain.

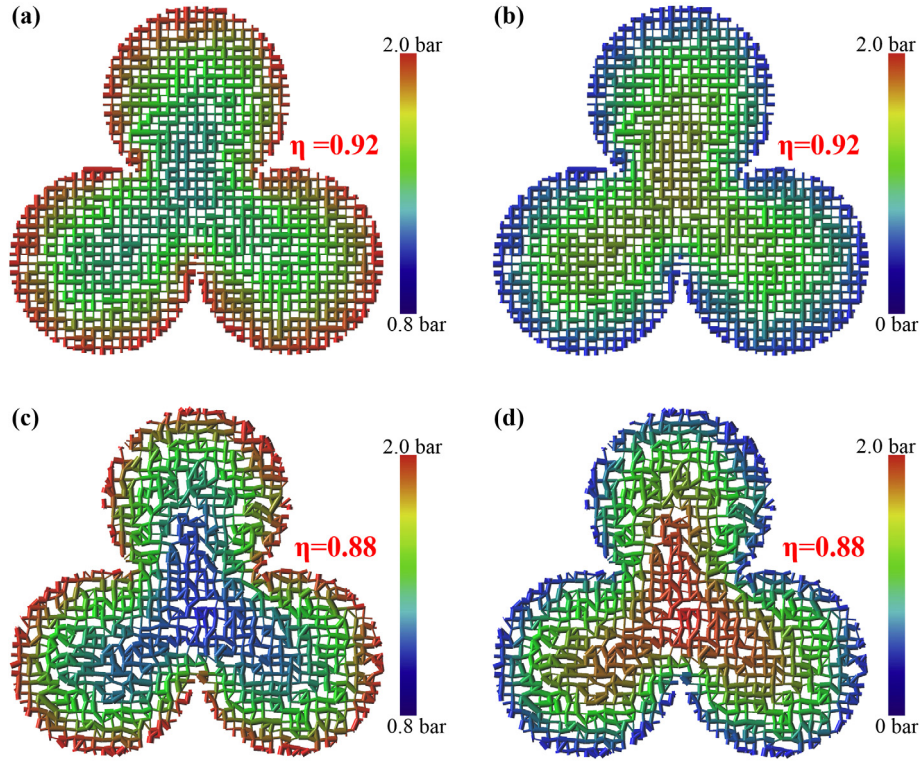

Fig. 8. Partial pressure profiles of (a) benzene and (b) cyclohexane in the T1R 2-D trilobe pore network; partial pressure profiles of (c) benzene and (d) cyclohexane in the T1IR 2-D pore network. The partial pressure profiles of hydrogen are presented in the Supporting Information.

Table 3
Effectiveness factors for pore networks with different external shapes.

Shapes	Dimensions	Characteristic particle length ($L_p = V/S$)	Effectiveness factor for regular pore network (η_R)	Effectiveness factor for irregular pore network (η_{IR})
Sphere	R = 5.5 mm (See Eq. (4))	1.83 mm	0.82	0.79
Cylinder	R = 4.2 mm, L = 12.6 mm (See Eq. (5))	1.57 mm	0.86	0.83
Hollow cylinder	R_1 = 7.2 mm, R_2 = 3.6 mm, L = 5.7 mm (See Eq. S4)	1.10 mm	0.96	0.94

are lower (see Table S1 in the Supporting Information), resulting in the relatively lower effectiveness factor. In addition, the difference in effectiveness factor between the two pore networks should be more significant when their connectivity is poor (e.g., $Z = 3$), according to the work of Hollewand and Gladden [7,8]. Therefore, to achieve a model with high accuracy, the pore-network randomness should be accounted for, even though the pore-network randomness is not as important as the connectivity in affecting conductivity [41–43].

4.3. Effect of pore-network external shape

By employing T1R and T1IR 3-D pore networks within a spherical, cylindrical, and hollow cylindrical (see Figs. 6a and c, 7a and c, S4a and c, respectively), the effect of the external shape on the performance of the catalyst particles is investigated. The dimensions of these shapes (see Table 3) are selected to achieve the same volume (i.e., 697 mm^3), hence the effect of particle volume on the performance of catalysts can be eliminated. The effectiveness factor increases with shape in the order: sphere < cylinder < hollow cylinder, and η_R is larger than η_{IR} for all the shapes, as shown in Table 3.

The generalized Thiele modulus (Φ), defined on the basis of a characteristic particle length ($L_p = V/S$) can be employed to explain the different effectiveness factors of the catalysts with different shapes [44], according to the η-Φ relation (η decreases with the increase of Φ).

$$\Phi = \frac{V}{S}\frac{r(P_{B,b})}{\sqrt{2}}\left[\int_{P_{B,e}}^{P_{B,b}} D_{eff} r(P_B) dP_B\right]^{-1/2} \tag{9}$$

Here, V and S are the volume and external surface area of the catalyst particle; r is the reaction rate; D_{eff} is the effective diffusivity; P_B is the partial pressure of benzene; $P_{B,e}$ is the partial pressure of benzene in equilibrium. In this work, since the gradients of temperature [20] and partial pressure of hydrogen (see Fig. S5 in the Supporting Information) can be assumed to be negligible, r is a function of only the partial pressure of benzene [45]:

$$r_i = \frac{v_i k P_B}{1 + K P_B} \tag{10a}$$

$$k = \frac{0.0199 \exp\left(\frac{-28250}{RT}\right)\left(\frac{P_{H,b}}{10}\right)^{0.5}}{\left[1 + 2.95 \times 10^{-2} \exp\left(\frac{-9370}{RT}\right)\left(\frac{P_{H,b}}{10}\right)^{0.5}\right]} \tag{10b}$$

$$K = 1.80 \times 10^{-5} \exp\left(\frac{41170}{RT}\right) \tag{10c}$$

Here, r_i and v_i are the reaction rate and stoichiometric number of component i, and R is the universal gas constant. The characteristic particle length decreases with shape in the order: sphere > cylinder > hollow cylinder (see Table 3), and, therefore, the effectiveness factor increases with shape in the same order according to Eq. (9) and the η-Φ relation. Since D_{eff} for a component in the T1R pore network is larger than the one in the T1IR pore network, as indicated in Section 4.2, the effectiveness factor for the regular pore network is larger than the one for the irregular pore network, according to Eq. (9) and the η-Φ relation. It should be noted that this Thiele modulus method may not be applicable when the kinetics are too complex (network of reactions) and the effective diffusivity changes with time (e.g., deactivation of the catalyst by coke).

5. Conclusions

In this work, a method was described to construct pore networks of arbitrary shape, provided that the shape of the domain can be described by a set of inequalities. The pore network cutting algorithm, which is the centrepiece of the method, was proposed to transform the square or cubic pore network skeletons into various shapes. By employing this pore network cutting algorithm, the original pore network skeletons can be reused infinitely, and this algorithm can be easily embedded into other methods for generating pore networks to transplant its 'pore network cutting' function. Pore networks with four 2-D shapes and four 3-D shapes were constructed as examples, and their corresponding domains were described by sets of inequalities. Then, some of these pore networks were applied to simulate hydrogenation of benzene to cyclohexane in porous catalysts. The simulation results show that the catalyst with the irregular pore network performs worse than the one with the regular network, because the irregular network has more tortuous diffusion paths. In addition, the effectiveness factor increases with pore-network shape in the order: sphere < cylinder < hollow cylinder, which is explained by the generalized Thiele modulus method. Therefore, to achieve a model with high accuracy, the pore-network randomness and shape should be accounted for.

The method proposed in this work adds external shape information of porous materials to pore networks, and expands the applications of pore networks to domains of arbitrary shape.

Acknowledgements

The authors are grateful for the financial support of the National Key Basic Research Program of China (2014CB239702), the National Natural Science Foundation of China (91434117 and 21376076), the China Postdoctoral Science Foundation (2016M600289), as well as support from the UK's EPSRC "Frontier Engineering" Centre for Nature Inspired Engineering (EP/K038656/1).

Appendix A. Supplementary data

Supplementary data associated with this article can be found, in the online version, at http://dx.doi.org/10.1016/j.cej.2017.02.036.

References

[1] S. Torquato, Random Heterogeneous Materials: Microstructure and Macroscopic Properties, Springer, New York, 2002.
[2] K. Vafai, Handbook of Porous Media, third ed., Taylor & Francis, Boca Raton, 2015.
[3] F.A.L. Dullien, Porous Media: Fluid Transport and Pore Structure, second ed., Academic Press, San Diego, 1992.
[4] K. Ishizaki, S. Komarneni, M. Nanko, Porous Materials: Process Technology and Applications, Springer, Dordrecht, 1998.
[5] M. Sahimi, G.R. Gavalas, T.T. Tsotsis, Statistical and continuum models of fluid-solid reactions in porous media, Chem. Eng. Sci. 45 (1990) 1443–1502.
[6] F. Keil, Diffusion and reaction in porous networks, Catal. Today 53 (1999) 245–258.
[7] M.P. Hollewand, L.F. Gladden, Modelling of diffusion and reaction in porous catalysts using a random three-dimensional network model, Chem. Eng. Sci. 47 (1992) 1761–1770.
[8] M.P. Hollewand, L.F. Gladden, Representation of porous catalysts using random pore networks, Chem. Eng. Sci. 47 (1992) 2757–2762.
[9] M.J. Blunt, Flow in porous media – pore-network models and multiphase flow, Curr. Opin. Colloid Interface Sci. 6 (2001) 197–207.
[10] M.J. Blunt, M.D. Jackson, M. Piri, P.H. Valvatne, Detailed physics, predictive capabilities and macroscopic consequences for pore-network models of multiphase flow, Adv. Water Resour. 25 (2002) 1069–1089.
[11] P. Rajniak, R.T. Yang, Unified network model for diffusion of condensable vapors in porous media, AIChE J. 42 (1996) 319–331.
[12] F. Jani, M. Dadvar, Three-dimensional pore network model of biofilter treating toluene: a study of the effect of the pore space morphology, Chem. Eng. Sci. 65 (2010) 3293–3300.
[13] C.L. Lin, J.D. Miller, Network analysis of filter cake pore structure by high resolution X-ray microtomography, Chem. Eng. J. 77 (2000) 79–86.
[14] T. Nukunya, J.S. Devinny, T.T. Tsotsis, Application of a pore network model to a biofilter treating ethanol vapor, Chem. Eng. Sci. 60 (2005) 665–675.
[15] M. El Hannach, J. Pauchet, M. Prat, Pore network modeling: application to multiphase transport inside the cathode catalyst layer of proton exchange membrane fuel cell, Electrochim. Acta 56 (2011) 10796–10808.
[16] M. Shahraeeni, M. Hoorfar, Pore-network modeling of liquid water flow in gas diffusion layers of proton exchange membrane fuel cells, Int. J. Hydrogen Energy 39 (2014) 10697–10709.
[17] R. Wu, Q. Liao, X. Zhu, H. Wang, Pore network modeling of cathode catalyst layer of proton exchange membrane fuel cell, Int. J. Hydrogen Energy 37 (2012) 11255–11267.
[18] J. Wood, L.F. Gladden, Modelling diffusion and reaction accompanied by capillary condensation using three-dimensional pore networks. Part 1. Fickian diffusion and pseudo-first-order reaction kinetics, Chem. Eng. Sci. 57 (2002) 3033–3045.
[19] J. Wood, L.F. Gladden, F.J. Keil, Modelling diffusion and reaction accompanied by capillary condensation using three-dimensional pore networks. Part 2. Dusty gas model and general reaction kinetics, Chem. Eng. Sci. 57 (2002) 3047–3059.
[20] G. Ye, X. Zhou, M.-O. Coppens, W. Yuan, Probing pore blocking effects on multiphase reactions within porous catalyst particles using a discrete model, AIChE J. 62 (2016) 451–460.
[21] G. Ye, X. Zhou, M.-O. Coppens, J. Zhou, W. Yuan, Influence of catalyst pore network structure on the hysteresis of multiphase reactions, AIChE J. 63 (2017) 78–86.
[22] J.-Y. Arns, V. Robins, A.P. Sheppard, R.M. Sok, W.V. Pinczewski, M.A. Knackstedt, Effect of network topology on relative permeability, Transp. Porous Med. 55 (2004) 21–46.
[23] A. Ebrahimi, S. Jamshidi, S. Iglauer, R.B. Boozarjomehry, Genetic algorithm-based pore network extraction from micro-computed tomography images, Chem. Eng. Sci. 92 (2013) 157–166.
[24] S. Jamshidi, R.B. Boozarjomehry, M.R. Pishvaie, Application of GA in optimization of pore network models generated by multi-cellular growth algorithms, Adv. Water Resour. 32 (2009) 1543–1553.
[25] M.E. Kainourgiakis, E.S. Kikkinides, A. Galani, G.C. Charalambopoulou, A.K. Stubos, Digitally reconstructed porous media: transport and sorption properties, Transp. Porous Med. 58 (2005) 43–62.
[26] C.A. Baldwin, A.J. Sederman, M.D. Mantle, P. Alexander, L.F. Gladden, Determination and characterization of the structure of a pore space from 3D volume images, J. Colloid Interface Sci. 181 (1996) 79–92.
[27] C.H. Arns, M.A. Knackstedt, K.R. Mecke, Characterisation of irregular spatial structures by parallel sets and integral geometric measures, Colloids Surf., A: Physicochem. Eng. Asp. 241 (2004) 351–372.
[28] A.R. Riyadh, T. Karsten, S.W. Clinton, Comparison of network generation techniques for unconsolidated porous media, Soil Sci. Soc. Am. J. 67 (2003) 1687–1700.
[29] H. Dong, M.J. Blunt, Pore-network extraction from micro-computerized-tomography images, Phys. Rev. E 80 (2009) 1–11.
[30] D. Silin, T. Patzek, Pore space morphology analysis using maximal inscribed spheres, Physica A 371 (2006) 336–360.
[31] J.S.S. Mohammadzadeh, A. Zamaniyan, Catalyst shape as a design parameter – optimum shape for methane-steam reforming catalyst, Chem. Eng. Res. Des. 80 (2002) 383–391.
[32] K.M. Brunner, H.D. Perez, R.P.S. Peguin, J.C. Duncan, L.D. Harrison, C.H. Bartholomew, W.C. Hecker, Effects of particle size and shape on the performance of a trickle fixed-bed recycle reactor for fischer-tropsch synthesis, Ind. Eng. Chem. Res. 54 (2015) 2902–2909.
[33] O. Šolcová, P. Schneider, Axial dispersion in single pellet-string columns with non-porous packing, Chem. Eng. Sci. 59 (2004) 1301–1307.
[34] O. Šolcová, K. Soukup, P. Schneider, Axial dispersion in single pellet-string columns packed with unusually shaped porous pellets, Chem. Eng. J. 110 (2005) 11–18.
[35] D. Wu, L. Song, B. Zhang, Y. Li, Effect of the mechanical failure of catalyst pellets on the pressure drop of a reactor, Chem. Eng. Sci. 58 (2003) 3995–4004.

[36] N.A. Idowu, M.J. Blunt, Pore-scale modelling of rate effects in waterflooding, Transp. Porous Med. 83 (2010) 151–169.
[37] G. Ye, X. Duan, K. Zhu, X. Zhou, M.-O. Coppens, W. Yuan, Optimizing spatial pore-size and porosity distributions of adsorbents for enhanced adsorption and desorption performance, Chem. Eng. Sci. 132 (2015) 108–117.
[38] Z. Cheng, A.M. Anter, G.M. Khalifa, J. Hu, Y. Dai, W. Yuan, An innovative reaction heat offset operation for a multiphase fixed bed reactor dealing with volatile compounds, Chem. Eng. Sci. 56 (2001) 6025–6030.
[39] Z. Cheng, A.M. Anter, W. Yuan, Intensification of phase transition on multiphase reactions, AIChE J. 47 (2001) 1185–1192.
[40] M.M. Mezedur, M. Kaviany, W. Moore, Effect of pore structure, randomness and size on effective mass diffusivity, AIChE J. 48 (2002) 15–24.
[41] P.H. Winterfeld, L.E. Scriven, H.T. Davis, Percolation and conductivity of random two-dimensional composites, J. Phys. C: Solid State Phys. 14 (1981) 2361–2376.
[42] G.R. Jerauld, J.C. Hatfield, L.E. Scriven, H.T. Davis, Percolation and conduction on Voronoi and triangular networks: a case study in topological disorder, J. Phys. C: Solid State Phys. 17 (1984) 1519–1529.
[43] G.R. Jerauld, L.E. Scriven, H.T. Davis, Percolation and conduction on the 3D Voronoi and regular networks: a second case study in topological disorder, J. Phys. C: Solid State Phys. 17 (1984) 3429–3439.
[44] K.B. Bischoff, Effectiveness factors for general reaction rate forms, AIChE J. 11 (1965) 351–355.
[45] Z. Zhou, Z. Cheng, Z. Li, W. Yuan, Determination of effectiveness factor of a partial internal wetting catalyst from adsorption measurement, Chem. Eng. Sci. 59 (2004) 4305–4311.